OPTICAL METHODS FOR LOCAL PULSE WAVE VELOCITY ASSESSMENT

T. Pereira, M. Cabeleira, P. Matos, E. Borges, V. Almeida, J. Cardoso, C. Correia

Instrumentation Center, Physics Department, University of Coimbra, R Larga, Coimbra, Portugal

H. C. Pereira

Instrumentation Center, Physics Department, University of Coimbra, Coimbra, Portugal
ISA- Intelligent Sensing Anywhere, Coimbra, Portugal

Keywords: Optical probes, Photodiode, Waveform distension, Pulse Transit Time, Pulse Wave Velocity.

Abstract: Pulse wave velocity (PWV) is a clinically interesting parameter associated to cardiac risk due to arterial stiffness, generally evaluated by the time that the pressure wave spends to travel between two arbitrary points. Optic sensors are an attractive instrumental solution in this kind of time assessment applications due to their truly non-contact operation capability, which ensures an interference free measurement. On the other hand, they can pose different challenges to the designer, mostly related to the features of the signals they produce and to the associated signal processing burden required to extract error free, reliable information. In this work we evaluate two prototype optical probes dedicated to pulse transit time (PTT) evaluation as well as three algorithms for its assessment. Although the tests were carried out at the test bench, where "well behaved" signals can be obtained, the transition to a probe for use in humans is also considered. Results demonstrated the possibility of measuring pulse transit times as short as 1 ms with less than 1% error.

1 INTRODUCTION

Pulse wave velocity (PWV) is defined as the velocity at which the pressure waves, generated by the systolic contraction of the heart, propagate along the arterial tree. PWV is a measure of regional arterial stiffness of the arterial territory between the two measurement sites. This parameter is related to the elastic modulus (E) of the arterial wall (which represents the intrinsic wall stiffness), and the arterial geometry (thickness: h) and blood density (ρ). The first relationship was formulated by Moens and Korteweg and expresses:

$$PWV = \sqrt{\frac{Eh}{d\rho}} \qquad (1)$$

Later on, Bramwell and Hill described (1) the association in terms of distensibility (D), which is determined by the blood vessel's compliance (C), the former relation can be expressed:

$$PWV = \frac{1}{\sqrt{\rho DC}} \qquad (2)$$

From the expression, we can deduce that higher PWV corresponds to lower vessel distensibility and compliance and therefore to higher arterial stiffness.

The pulse waves travel through the arteries at a speed of 4 to 10 meters per second depending on the vessel (PWV increases with the distance from the heart), and the elastic condition of the arterial wall, which is affected by a variety of factors in health and disease (Bramwell, 1922; Nichols, 2005).

The most common technique to assess non-invasively PWV is based on the acquisition of pulse waves generated by the systolic ejection at two distinct locations, separated by a distance d, and determination the time delay, or pulse transit time, due to the pulse wave propagation along the arterial tree (Rajzer, 2008). The PWV parameter is then simply calculated as the linear ratio between d and the PTT.

Many different pulse waves have been used to assess pulse wave velocity, such as pressure wave, distension wave or flow wave. The gold standard in PWV assessment uses pressure waves measured by pressure sensors (Laurent, 2006). These sensors need to exert pressure in the blood vessel this will distort the waveform, and may lead to inaccurate measurements. Another drawback of this method is the fact that the predicted PWV is relative to a large extension of the arterial tree and therefore is the conjunction of different local PWVs.

Other studies describe ultrasonic probes that predict PWV using Doppler Effect and modified ecography probes (Minnan Xu, 2002), but the PWV measurements were unreliable.

Recently (Kips *et al*, 2010; Vermeersch *et al*, 2008), described alternative approaches for estimating carotid artery pressures with an ultrasound system. Calibrated diameter distension waveforms were compared to the more common approach based on pressure waves, proving to be a valid alternative to local pressure assessment at the carotid artery.

All the previous techniques are minimally invasive, but the probe has to be in contact with the patient's tissues at the artery site. This contact, as stated above, can distort the signal integrity and thus rise the interest in exploring true non-contact technique.

The propagation of pressure waves in arterial vessels generates distensions in the vessel's walls. These distensions can be optically measured in peripheral arteries like the carotid that, as they run very close to the surface impart a visible distention. This distention, as it modulates the reflection characteristics of the skin, can be used to generating an optical signal correlated with the passing pressure wave.

The probes developed in this work, gather the light generated by LED illumination and reflected by the skin, using two photodiodes placed 3 cm apart, all assemble in a single probe. PWV is assessed by measuring the time delay between the signals of the two photo-sensors using different algorithms that are also discussed.

2 TECNOLOGIES

Two distinct types of silicon optical sensors – planar and avalanche photodiode (APD) – are used in this work, each one requiring a particular electronic circuitry. Results, however, are derived by the same signal processing algorithms.

Each probe incorporates two identical optical sensors placed 3 cm apart and signal conditioning electronics based on a transconductance amplifier and low-pass filter. The APD probe includes the high voltage biasing circuitry (250V) necessary to guarantee the avalanche effect. Illumination is provided by local, high brightness, 635 nm light-emitting diodes (LEDs).

A photodiode (PD) is a type of photo-detector with the ability of converting light into either current or voltage, according to the *modus operandi*. One decided to use a planar, rectangular-shaped photodiode, its dimensions being 10.2x5.1mm. This is silicon solderable photodiode feature low cost, high reliability and a linear short circuit current over a wide range of illumination.

Analogously to the conventional photodiodes, APDs operate from the electron-hole pairs created by the absorption of incident photons. The high reverse bias voltage of APDs, however, originates a strong internal electric field, which accelerates the electrons through the silicon crystal lattice and produces secondary electrons by impact ionization. This avalanche effect is responsible for a gain factor up to several hundred.

APDs are operated with a relatively high reverse voltage and will typically require 200 to 300 volts of reverse bias. Under these conditions, gains of around 50 will result from the avalanche effect, providing a larger signal from small variations of light reflected from the skin and will, at least theoretically, improve the signal-to-noise ratio (SNR).

On the other hand, since the sensitive area of this sensor is very small (1 mm^2), the accuracy of the estimations increases. In fact, comparatively to the planar photodiode, in which the detection of light takes place over a much larger area, this sensor can measure an almost punctual section of the skin, thus decreasing the error associated to the detection solid angle.

The two prototype probes, on which we support this work, incorporate an APD from Adavanced Photonics (SD 012-70-62-541) and a planar type from Silonex (SLCD-61N3) respectively.

3 TEST SETUP

The test setup was designed to assess the two main parameters of in PWV measurements: linearity and time resolution.

Their assessment was carried out in a test setup where illumination is provided by two LEDs whose light intensities reproduce the same signal with a

variable time delay between them, as shown in Figure 1.

Two arbitrary waveform generators, Agilent 33220A (AWG1 and AWG2), are synchronously triggered by an external signal. The waveform generators have been previously loaded with the same typical cardiac waveforms and the mutual delay is selected in order to simulate different pulse transit times (Figure 2). These signals must be added to a small offset of the order of the magnitude of the forward voltage drop of the LED, so that the resulting light intensity is linearly modulated by the LED signal current. A 16-bit resolution data acquisition system (National Instruments, USB6210) samples the signals at a 20 kHz rate, adequate for PTTs as low as 100 µs and stores them for off-line analysis using MatlabTM.

Figure 3 shows a typical set of signals generated and detected by the circuit of Figure 1.

Figure 3: Excitation and detector responses for a) Planar Photodiode b) Avalanche Photodiode.
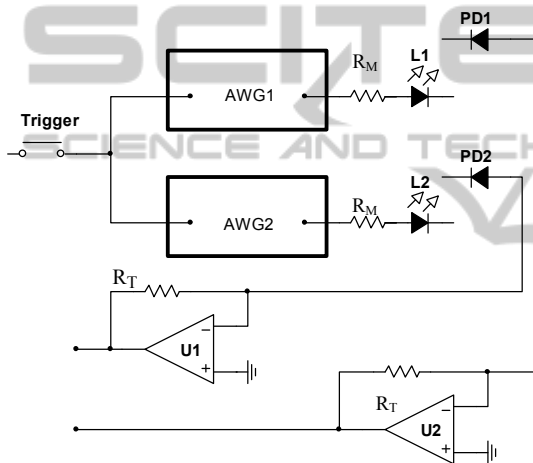
Figure 1: Light modulation and detection circuit.

In the test setup, the probe is placed in front of a test device, see Figure 2, which holds the two modulated LEDs and provides light isolation to prevent crosstalk. During the tests, the LEDs of the probe itself are deactivated and all light comes from the LEDs in the test device.
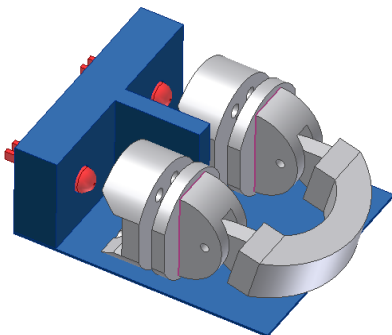

Figure 2: During test, the probe is held to the blue part. The test LEDs activated by circuit of Figure 1.

To assess the operational limits of our probes and algorithms, we designed three different tests. In the first one, signals with frequency similar to the normal heart rate but with delays within the interesting PTT range are fed to the system to investigate the integral linearity error. This test was performed at a constant frequency of 1.5 Hz and time delays varying from 1ms to 100ms, corresponding to PWVs in a 30m/s to 0.3m/s interval. This range of values includes the normal PTT range of values in humans.

In the second test we assess the robustness of the algorithms to noise. To do this, we add white noise of amplitudes ranging from 1% to 50% of the signal amplitude in 0.02% steps, to the isolated pair of pulses. For each noise level, 1000 samples produced in order to obtain reasonable statistics. The resulting PTT distribution is then studied.

The third test was intended to validate our algorithm's operability under a wide range of frequencies (simulating different Heart rates) with a time lag far greater than the maximum PTT seen in humans. It consisted of varying the output frequency (1 Hz to 200 Hz) of the cardiac pulses keeping the time lag between the two signals at 1.1ms.

4   SIGNAL PROCESSING

Three different algorithms for extracting the time delay from the detector's signals are considered. They are referred to as foot-to-foot, cross-correlation and phase spectra. Their basis derives from the homonymous mathematical functions.

The accuracy of the results delivered by the algorithms discussed in this section is compared with the reference delay selected at the waveform generators.

In the foot-to-foot method and in spite of more complex methods (Kazanavicius, 2005), a simple detection of the time lag between the start of the upstroke of the two consecutive pulses is carried out. This is possible due to the well behaved nature and low noise levels of our signals. A different situation occurs in signals collected from a patient, mostly due to baseline drift.

The cross-correlation method is based on the well known property of the peak of cross-correlogram that allows delays to be calculated by subtracting the peak time position from the pulse length (Azaria, 1984). Two different correlation functions are used: one that belongs to the MatlabTM core (*Xcorr*) and another one that generates the cross-correlation making direct use of the cross-correlation theorem (*Fcorr*).

The third method uses data in the phase spectra of the signals. In this method, we first identify the exact frequency of the signal's harmonics, using the amplitude spectra, and then, extract the corresponding phase angles from the phase spectra.

The phase angle, θ, is related with angular frequency of the phase spectrum, ω and with the time delay, t, according to:

$$\theta = \omega \cdot t \qquad (3)$$

On its turn, the time delay is computed from the phase angles of the same harmonic in the phase spectra of each signal, θ_1 and θ_2:

$$t = \frac{(\theta_1 - \theta_2)}{\omega} \qquad (4)$$

Despite the fact that, theoretically, the time delay can be determined at any harmonic of the complete spectrum, the practice, however, differs, given their affectation by noise. Nevertheless, by performing the filtering at the detector amplifier level, one is able to obtain a lower error, as long as the best harmonics (that is, with the highest SNR possible) are selected. For the circuits used in this study, one checked best performances when the time delay was

computed at the 2nd harmonic in the APD case and in the 4th one for the PP circuits.

5   RESULTS

This section is dedicated to the discussion of results obtained with the two probes using the previously mentioned algorithms.

5.1   Integral Linearity

By definition, integral linearity is the maximum deviation of the results from the reference straight line, expressed as a percentage of the maximum. We explore delays in the 1 to 100 ms interval. Results are shown in Figures 4 and 5.

A higher number of points are taken close to the origin since this is the interesting range of values in human PTT studies using the optical probes.
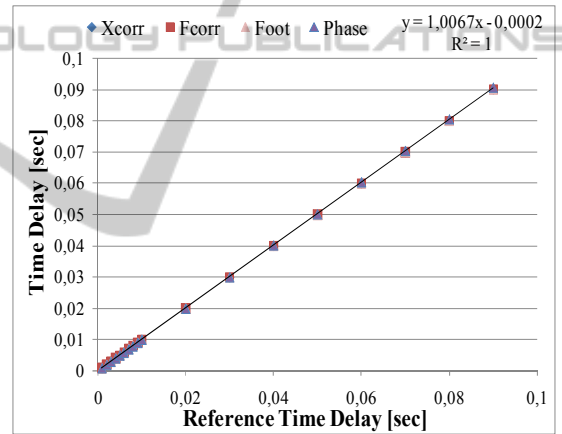

Figure 4: Reference Delay versus measured delay for the PP probe. The APD curve practically coincides with this one.

For both probes, all the algorithms produce highly linear (better than 1%) results as well as low error agreement with the reference time delay.

5.2   PTT Error

Error plots, expressed as a percentage of the corresponding reference value, are shown in Figures 5 and 6. We discuss the main differences between the PP and the APD probes.
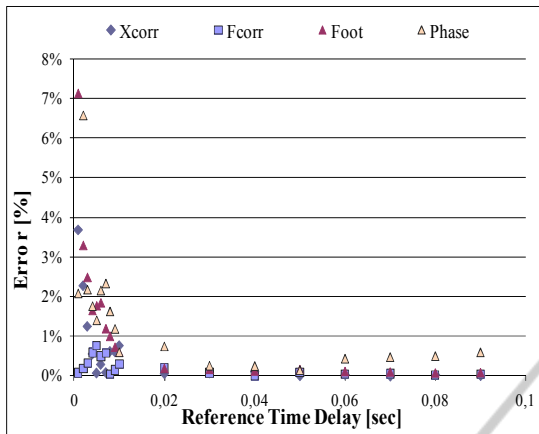
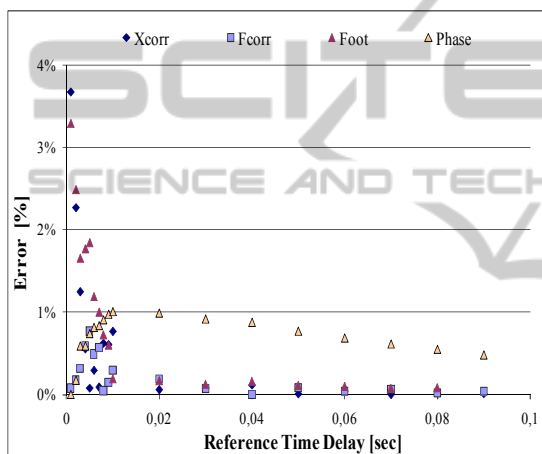Figure 5: Relative errors by algorithm, for the PP probe.

Figure 6: Relative errors, by algorithm, for the APD probe.

While the PP probe exhibits lower than 8% error, the APD one never exceeds the 4% limit.

Cross-correlation (*Fcorr* version) can be identified as the best performing algorithm with a relative error never exceeding 1% in any probe.

In the APD probe, the phase angle detection method also yields very good (lower than 1%) error, but poor performance for the PP probe, mainly in the small time lag region.

As expected all the algorithms performed almost perfectly for higher than 10ms time delays.

5.3 Noise Tolerance

Robustness of the algorithms to noise is assessed by adding normal distribution noise to the photodiode readings and studying the resulting effect on the algorithm output.

This test was performed just for the correlation and phase methods. It was not used in foot-to-foot detection, because, as long as added noise is of the order of magnitude of the threshold used to detect the upstroke, the upstroke will not be detected at all.

Data collected by the PP and APD probes was submitted to this test using the following procedure: for each noise level, the algorithm under test was run 1000 times, with an independent noise vector affecting every run.

In total, 25 relative noise levels, from zero to 0.5 of peak amplitude, were explored.

Figures 7 to 12, enclosing the full information of this test, are shown side by side to make comparisons easier.

Figures 8 and 9 show the dispersion introduced by noise for a reference delay of 4.1 ms. The resulting PTT values, taken as the mean value of each distribution, are plotted in Figure 9. While these figures concern the PP probe, Figures 10, 11 and 12 represent the same study for the APD probe.

As mentioned before, noise is expressed as a fraction of the peak amplitude of the signal.
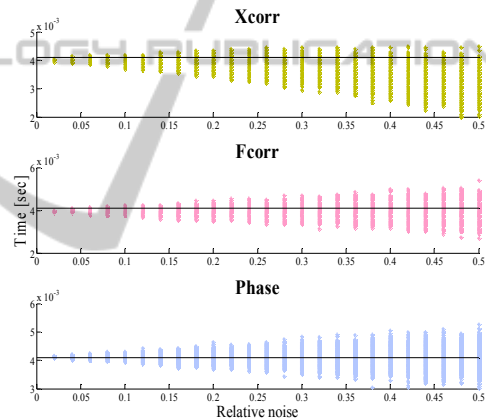

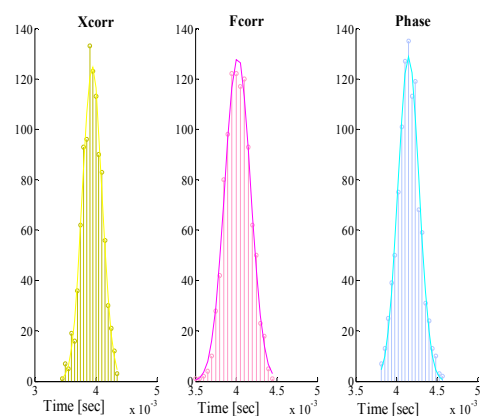Figure 7: Dispersion introduced by noise in the PP probe.

Figure 8: PTT dispersion plots for each algorithm, for a relative noise level of 0.14. The gaussian fittings stress the normal nature of the distributions.
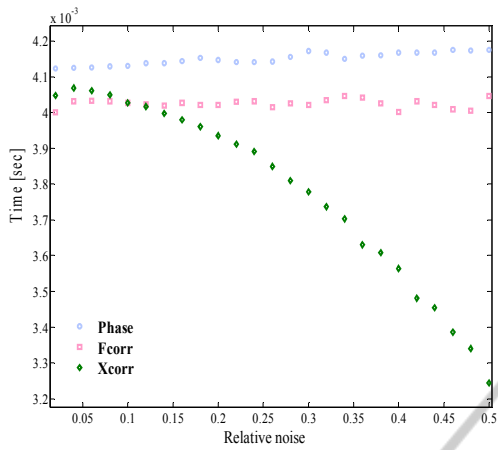
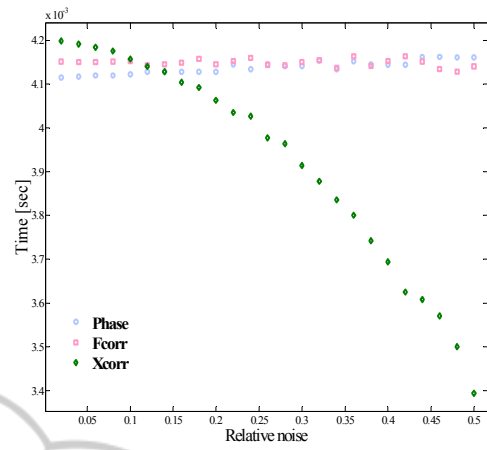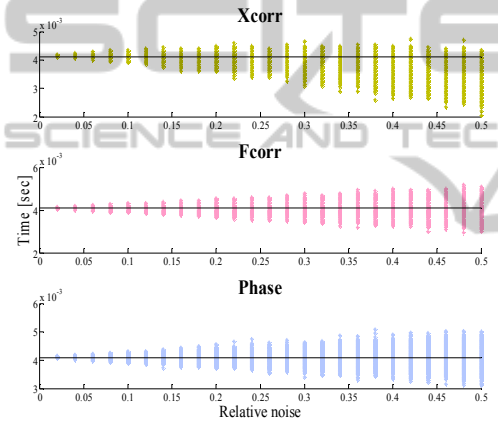Figure 9: Mean of distribution vs. relative noise for a 4.1 ms reference delay in the PP probe.

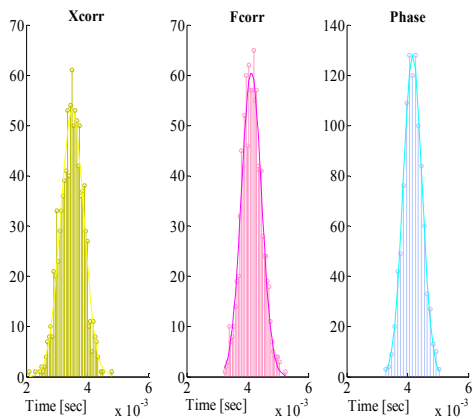Figure 10: Dispersion introduced by noise for the APD probe.

Figure 11: PTT dispersion plots for each algorithm, for a relative noise level of 0.14. The gaussian fitting stresses the normal nature of the distribution.

Figure 12: Mean of distribution vs. relative noise for a 4.1 ms reference delay in the APD probe.

Not surprisingly, the dispersion introduced by adding noise is also gaussian with variance proportional to the noise level (Figures 8 and 11).

However, different robustness to noise is exhibited by each of the three tested algorithms, with the phase and *Fcorr* methods showing the lowest errors when subject to high levels of noise.

It is also clear that the *Xcorr* based algorithm is not robust to noise and, under high noise conditions it shows a strong tendency to under-evaluate PTT, as shown in Figures 9 and 12.

The phase method exhibits the higher levels of robustness since its median remains constant for high noise levels and, in addition, the corresponding distribution shows the lower variance. The large offset yielded by this algorithm in the PP probe (but not in the APD probe) is rather puzzling and is probably associated to the particular shape of PP signals which, very much unlike the APD, are conditioned by the large equivalent capacity of the photosensor.

Another clarifying way to look at the overall performance of probes and algorithms is shown in Figure 13 where the probabilities of the algorithm returning a PTT value with less than 5% and less than 10% error are plotted against noise. Results, expressed as a percentage, are derived from 1000 runs per curve.

Data in Figure 13 confirms the superior robustness of the phase method.
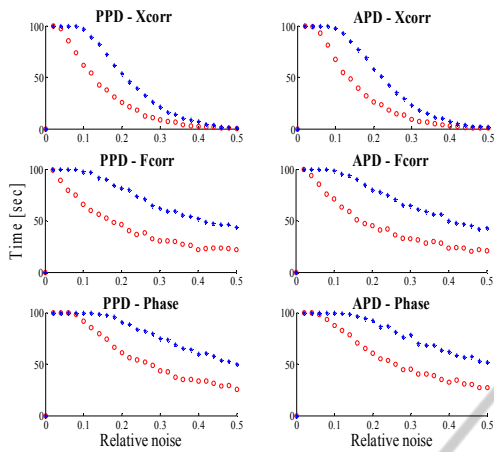
Figure 13: Measurements with less than 5% error (blue dots) and less than 10% error (red circles) vs. relative noise.

As can be stated, all algorithms can deliver 100% measurements within the specified error threshold, up to a certain noise level, where the curves show a turning point and start decaying towards zero. The phase algorithm not only shows a higher turning point but also decays much slowly as noise increases, denoting extra robustness to noise.

5.4 Algorithm Robustness

A final test was carried out in order to study the effect of different heart rates on the performance of the algorithms. In fact, all the data mentioned so far was acquired at a rate of 1 pulse per second, thus, any conclusive notes might not be valid for other acquisition rates. Accordingly, the referred test was performed for signal repetition rates varying from 1 to 200 Hz, without artificial noise added to the readings and for a known constant time delay.
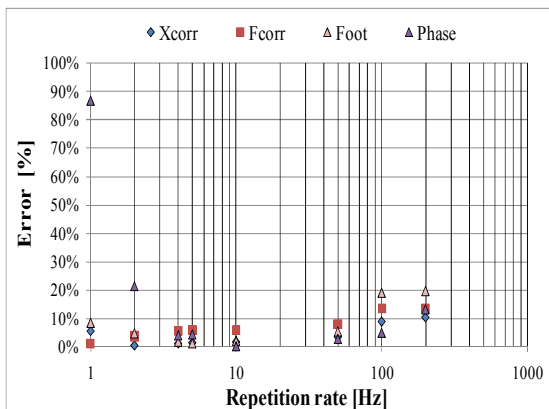

Figure 14: Plot of the relative errors for each algorithm for a range of frequencies of signal, for the PP probe.
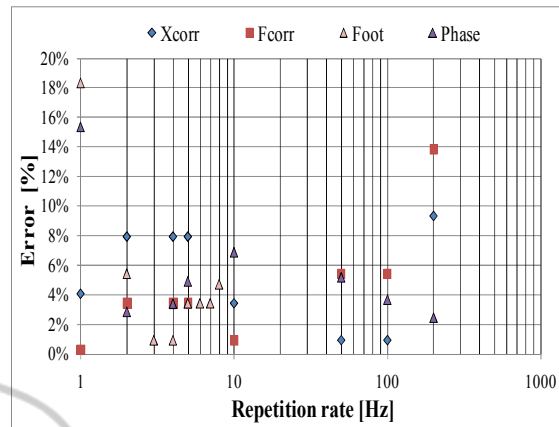

Figure 15: Plot of the relative errors for each algorithm for a range of frequencies of signal, for the APD probe.

The value used for the time delay, 1.1 ms, was selected by mere convenience. At this point it's not unimportant to remark that the AWG2 (Figure 1) can define the time delay as an angle, the *delay angle*, with a precision of a tenth of a degree; on the other side, for the specific used set of repetition rates, the value of 1.1 ms yields feasible values for delay angles that, otherwise, could not be loaded by the equipment.

In conclusion, as Figures 14 and 15 reveal, the APD probe performs superiorly (note that the vertical scales of the figures are different). It is also noticeable that the *Fcorr* and the phase algorithms produce the best results if the entire range of repetition rates is considered.

6 CONCLUSIONS

Two optical probes specifically designed to measure PTT have been developed and tested along with three different signal processing algorithms.

Tests show that although both probes are capable of measuring PTT accurately, the APD based one is more precise and accurate.

All three tested algorithms can measure PTT with an error below 8%. Nevertheless, just the one designated by *Fcorr* exhibits the capability of measuring PTT with an error bellow 1%, for the complete range of delays. The phase method shows the higher levels of robustness to noise.

When the signal repetition rate spans over a large range of values, the *Fcorr* algorithm can deliver PTTs with the lowest errors.

The natural follow-up of this work will be start acquiring pulse data in humans. Figure 16 shows a preliminary acquisition in human using the APD

probe. The shape of the pulses is very clear, not to much affected by noise and allows the anticipation of good results.
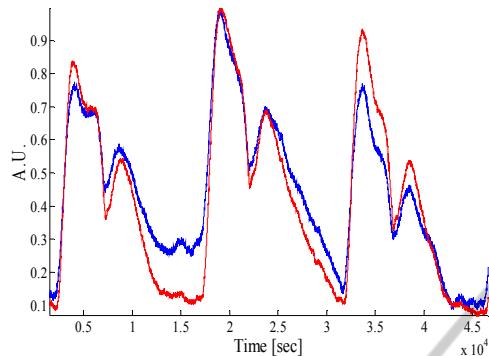

Figure 16: Preliminary results of the APD probe acquiring data in humans.

ACKNOWLEDGEMENTS

REFERENCES

Laurent S, et al., 2006. Expert consensus document on arterial stiffness: methodological issues and clinical applications Eur Heart. J. 27 2588-2605.

Kips J, et al., 2010. The use of diameter distension waveforms as an alternative for tonometric pressure to assess carotid blood pressure. *Physiol. Meas*. 31 (2010) 543–553.

Vermeersch S. J. et al., 2008. Determining carotid artery pressure from scaled diameter waveforms: comparison and validation of calibration techniques in 2026 subjects. *Physiol. Meas*. 29 1267–80.

Minnan Xu, 2002 Local Measurement of the Pulse Wave Velocity using Doppler Ultrasound. *Massachusetts Institute of Tecnology*.

Bramwell J. and Hill A., 1922. The velocity of the pulse wave in man. Proc Roy Soc Lond [Biol]. 93 298-306

Nichols, W. and O'Rourke, M. F., 2005. McDonald's Blood Flow in Arteries: Theoretical Experimental and Clinical Principles. 5th ed., London.

Rajzer M. et al., 2008. Comparison of aortic pulse wave velocity measured by three techniques: Complior, Spymocor and Arteriograph. J. Hypertens. 26 2001:2007.

Azaria M. and Hertz D., 1984. Time delay estimation by generalized cross correlation methods. *IEEE Trans. Acoustics, Speech, and Signal Processing*, vol. ASSP-32, pp. 280-285.

Kazanavicius E. and Gircys R., 2005. Mathematical Methods for determining the foot point of the Arterial Pulse Wave and Evaluation of Proposed Methods. *ISSN 1392 – 124X Information Technology and Control*.